

1 *Research Report*

2

3 **Phosphorylation and ubiquitination independent endocytosis of BRI1**

4

5 Lucas Alves Neubus Claus,^{1,2,10} Derui Liu,^{1,2,7,10} Ulrich Hohmann,^{3,8} Nemanja Vukašinović,^{1,2}
6 Roman Pleskot,^{1,2,9} Jing Liu,⁴ Alexei Schiffner,⁵ Yvon Jaillais,⁶ Guang Wu,⁴ Sebastian Wolf,⁵
7 Daniël Van Damme,^{1,2} Michael Hothorn,³ and Eugenia Russinova^{1,2*}

8

9 ¹Department of Plant Biotechnology and Bioinformatics, Ghent University, 9052 Ghent,
10 Belgium

11 ²Center for Plant Systems Biology, VIB, 9052 Ghent, Belgium

12 ³Structural Plant Biology Laboratory, Department of Botany and Plant Biology, University of
13 Geneva, 1211 Geneva, Switzerland

14 ⁴College of Life Sciences, Shaanxi Normal University, Xi'an, Shaanxi, 710062, P.R. China

15 ⁵Center for Plant Molecular Biology (ZMBP), University of Tübingen, 72076 Tübingen,
16 Germany

17 ⁶⁵Laboratoire Reproduction et Développement des Plantes (RDP), Université de Lyon, Ecole
18 Normale Supérieure de Lyon, Centre National de la Recherche Scientifique (CNRS), Institut
19 National de Recherche pour l'Agriculture, l'Alimentation et l'Environnement (INRAE),
20 69342 Lyon, France

21 ⁷Present address: College of Life Sciences, Shandong Agricultural University, Tai'an 271018,
22 China

23 ⁸Present address: Institute of Molecular Biotechnology of the Austrian Academy of Sciences
24 (IMBA) & Institute of Molecular Pathology (IMP), Vienna BioCenter (VBC), 1030 Vienna,
25 Austria

26 ⁹Present address: Institute of Experimental Botany, Academy of Sciences of the Czech
27 Republic, 16502 Prague 6, Czech Republic

28 ¹⁰These authors contributed equally

29 *Correspondence: eugenia.russinova@psb.vib-ugent.be

30

31 **Abstract**

32

33 The brassinosteroid (BR) hormone and its plasma membrane receptor BR INSENSITIVE1
34 (BRI1) is one of the best-studied receptor-ligand pairs for understanding the interplay
35 between receptor endocytosis and signaling in plants. BR signaling is mainly determined by
36 the plasma membrane pool of BRI1, whereas BRI1 endocytosis ensures signal attenuation.
37 Since BRs are ubiquitously distributed in the plant, the tools available to study BRI1 function
38 without interference from endogenous BRs are limited. Here, we designed a BR-binding-
39 deficient mutant based on protein sequence-structure analysis and homology modeling of
40 BRI1 and its close homologues. This new tool allowed us to re-examine the BRI1 endocytosis
41 and signal attenuation model. We show that despite decreased phosphorylation and
42 ubiquitination, the BR-binding-deficient BRI1 was internalized similar to the wild type form.
43 These results reinforce the hypothesis that BRI1 is internalized via parallel endocytic routes
44 and machineries. In addition, BR-binding-deficient mutant provides opportunities to study
45 non-canonical ligand-independent BRI1 functions.

46

47 **Keywords**

48

49 BRI1, brassinosteroids, ligand-binding, endocytosis, non-canonical

50

51 **Introduction**

52

53 Brassinosteroids (BRs) are low abundant and ubiquitously distributed plant steroidal
54 hormones that play essential role in growth, development, immunity and responses to stress
55 (Nolan et al., 2020). BR biosynthetic or signaling mutants display severe phenotypes
56 including dwarfism, dark-green leaves, photomorphogenesis in the dark, and late flowering
57 (Nolan et al., 2020). BRs are perceived at the cell surface by a leucine-rich repeat (LRR)
58 receptor kinase BR INSENSITIVE1 (BRI1) (He et al., 2000; Hothorn et al., 2011; Kinoshita
59 et al., 2005; She et al., 2011; Wang et al., 2001) . BR binding triggers the dissociation of the
60 inhibitory proteins BRI1 KINASE INHIBITOR1 (BKI1) and BAK1-INTERACTING
61 RECEPTOR-LIKE KINASES3 (BIR3), allowing interaction between BRI1 and its coreceptor
62 BRI1-ASSOCIATED KINASE1 (BAK1), which is required for downstream signaling
63 (Hohmann et al., 2018a; Li et al., 2002; Wang and Chory, 2006). BR signal is conveyed from
64 the cell surface to the nucleus through a sequence of phosphorylation/de-phosphorylation
65 events that activate the transcription factors of the BRASSINAZOLE-RESISTANT1 (BZR1)
66 and BRI1-EMS-SUPPRESSOR1 (BES1)/BZR2 family (Wang et al., 2002; Yin et al., 2002;
67 Chen et al., 2019). BRI1 receptor functions go beyond its canonical BR signaling function as
68 together with the RECEPTOR-LIKE PROTEIN44 (RLP44) and BAK1, BRI1 controls xylem
69 cell fate independently of BRs (Holzwart et al., 2018, 2020).

70 An important regulatory step in BR signaling is the control of the plasma membrane
71 (PM) pool of BRI1, which is determined by BRI1 endocytosis, recycling, and secretion (Irani
72 et al., 2012; Luo et al., 2015). As a consequence, impaired endocytosis or receptor secretion,
73 enhanced and reduced BR signaling, respectively (Irani et al., 2012; Luo et al., 2015). Several
74 studies have focused on BRI1 dynamics upon ligand binding. Given that exogenous BRs did
75 not change BRI1 internalization dynamics, BRI1 endocytosis was described as ligand-
76 independent (Geldner et al., 2007; Luo et al., 2015; Russinova et al., 2004). Subsequent
77 studies on post-translation modifications (PTM) showed that BRI1 undergoes
78 polyubiquitination that is mediated by the plant U-box (PUB) E3 ubiquitin ligases PUB12 and
79 PUB13 and requires BR binding (Zhou et al., 2018). BRI1 ubiquitination is a signal for BRI1
80 endocytosis and vacuolar sorting, since disruptions in this process by mutations in either the
81 ubiquitination sites or the E3 ligases translate into accumulation of BRI1 in the PM and
82 consequently BR sensitivity increases (Martins et al., 2015; Zhou et al., 2018).

83 Available tools used to study the dependence of BRI1 trafficking on ligand-binding
84 are limited and rely on the depletion of the endogenous BRs by using BR biosynthetic
85 mutants or the BR biosynthesis inhibitor, brassinazole (BRZ) (Asami et al., 2000). However,
86 the possibility cannot be excluded that treatment with BRZ might not completely deplete
87 bioactive BRs and that the BR biosynthetic mutant might contain biologically active BR
88 precursors. Furthermore, BR biosynthetic mutants display pleiotropic phenotypes that could
89 lead to general changes in membrane trafficking. Therefore, the use of these tools could
90 hamper analysis of ligand-independent BRI1 dynamics.

91 Here, we report the characterization of a quintuple (Q) BR binding-deficient BRI1
92 receptor mutant, designated as BRI1^Q, that was generated using homology and structure
93 analysis of BRI1 and its three homologues BRI1-LIKE1 (BRL1), BRL2 and BRL3 (Caño-
94 Delgado et al., 2004). This new tool revealed that BRI1 endocytosis is largely independent of
95 BRs and despite strongly decreased phosphorylation and ubiquitination the BRI1^Q mutant
96 held normal endocytosis rates. These results reinforce the hypothesis that BRI1 is internalized
97 via parallel endocytic routes and machineries. Moreover, we used the BRI1^Q mutant to
98 investigate BR-independent BRI1 functions, such as xylem cell differentiation. We showed
99 that BRI1^Q can partially complement the xylem cell fate phenotype of the *bri1* null mutant,
100 suggesting that BRI1^Q can be used to study BRI1 non-canonical functions.

101

102 **Results and Discussion**

103

104 **BRI1^Q cannot bind BRs**

105 The *Arabidopsis thaliana* (Arabidopsis) genome encodes for three BRI1 homologs,
106 designated BRL1, BRL2 and BRL3, of which BRL2 does not bind BRs (Caño-Delgado et al.,
107 2004; Kinoshita et al., 2005). Sequence analyses of BRI1, BRL1, BRL2 and BRL3
108 ectodomains (Figure 1A) and examination of the crystal structure of the BRI1 ectodomain in a
109 complex with brassinolide (BL), the most active BR (Hothorn et al., 2011; She et al., 2011;
110 Wang et al., 2001) (Figure 1B-1D), revealed five putative residues important for BR binding,
111 three derived from changes in the BRL2 sequence [tyrosine (Y)597, Y599 and methionine
112 (M)657] and two bulky hydrophobic residues located at a 4 Å distance from the BL molecule
113 in BRI1 [Y642 and phenylalanine (F)681] (Figure 1B and 1C). Y597, Y599 and Y642 map to
114 the inner surface of the BRI1 island domain, forming the distal part of the BR-binding pocket,
115 whereas M657 and F681 are located in the LRR core and establish hydrophobic interactions

116 with the aliphatic BL moiety (Figure 1B and 1C). The identified residues were mutated to the
117 corresponding ones in BRL2 either individually ($\text{BRI1}^{\text{Y599F}}$ and $\text{BRI1}^{\text{M657E}}$) or in a
118 combination ($\text{BRI1}^{\text{Y597M/Y599F/M657E}}$) or to alanine (A) ($\text{BRI1}^{\text{Y597A/Y599A/M657A}}$). Finally, a
119 quintuple $\text{BRI1}^{\text{Y597M/Y599F/Y642A/M657E/F681A}}$ version was generated and designated as BRI1^{Q} .
120 Next, the binding kinetics of BL to the BRI1^{Q} ectodomain was determined by grating-coupled
121 interferometry (GCI) (Figure 2B). As controls, the ectodomains of wild type BRI1 and that of
122 the previously characterized in *bri1-6* mutant that carries the glycine (G) 644 to asparagine
123 (D) missense mutation ($\text{BRI1}^{\text{G644D}}$) were included (Hohmann et al., 2018a; Hothorn et al.,
124 2011; Kinoshita et al., 2005; Noguchi et al., 1999; Wang et al., 2001). Analytical size-
125 exclusion chromatography and right-angle light scattering experiments confirmed that all
126 BRI1 variants were monodisperse, suggesting that mutations in the BR-binding pocket do not
127 affect the overall shape and oligomeric state of the BRI1 ectodomain (Figure S1). The GCI
128 experiments revealed that BRI1 bound BL with a dissociation constant (K_D) of ~ 10 nM as
129 previously reported (Hohmann et al., 2018a; Wang et al., 2001), BRI1^{Q} did not bind BL,
130 whereas the $\text{BRI1}^{\text{G644D}}$ mutant displayed a strongly reduced BL-binding capacity with a K_D of
131 ~ 11.6 μM .

132 After confirmation that BRI1^{Q} cannot bind BL, mutated full-length BRI1 versions
133 fused to mCitrine (mCit) were expressed in the *bri1* null mutant from the native promoter and
134 plants with similar protein expression levels of the transgenes were selected (Figures 2A and
135 S2A). $\text{BRI1}^{\text{Y599F}}$ -mCit, $\text{BRI1}^{\text{M657E}}$ -mCit and $\text{BRI1}^{\text{Y597M/Y599F/M657E}}$ -mCit partially
136 complemented the *bri1* dwarf phenotype and localized in the PM and in intracellular punctate
137 structures, similar to the wild type BRI1 (Geldner et al., 2007; Russinova et al., 2004) (Figure
138 2A). By contrast, $\text{BRI1}^{\text{Y597A/Y599A/M657A}}$ -mCit and BRI1^{Q} -mCit did not complement the *bri1*
139 mutant (Figure 2A). The reason for the lack of *bri1* complementation by
140 $\text{BRI1}^{\text{Y597A/Y599A/M657A}}$ -mCit was the aberrant localization of this BRI1 mutant isoform in the
141 vacuole. BRI1^{Q} -mCit, however, exhibited the correct BRI1 localization in the PM and in
142 intracellular punctate structures. Hence, the absence of BRI1^{Q} functionality corroborates the
143 *in vitro* ligand-binding deficiency results (Figure 2B). To further characterize the BRI1^{Q} -mCit
144 line, we tested the BL-induced BRI1 PTMs. It is well established that after ligand binding,
145 BRI1 heterodimerizes with its co-receptor BAK1 and undergoes PTMs such as
146 phosphorylation and ubiquitination (Belkhadir and Jaillais, 2015; Martins et al., 2015; Zhou et
147 al., 2018). Moreover, BL treatment promotes the dephosphorylation of the transcription factor
148 BES1 in a dose-dependent manner, which is frequently used as a BR signaling indicator (Yin

149 et al., 2002). In agreement with the impaired BL binding, BRI1^Q-mCit had no detectable
150 phosphorylation, ubiquitination, did not interact with BAK1 and did not promote BES1
151 dephosphorylation after BL treatment (Figure 2C and 2D). These findings indicate that BRI1^Q
152 is unable to perceive BRs.

153

154 **Endocytosis of BRI1 is independent of BR binding**

155 The lack of BL binding in the BRI1^Q mutant provides a powerful tool to investigate different
156 aspects of BRI1 regulation, including endocytosis, without interference from BRs. Although
157 initially BRI1 endocytosis had been described as ligand independent (Geldner et al., 2007;
158 Russinova et al., 2004), later BR perception has been demonstrated to promote BRI1
159 ubiquitination (Zhou et al., 2018), which assists BRI1 internalization and vacuolar targeting
160 (Luo et al. , 2022; Martins et al., 2015; Zhou et al., 2018). We revisited the BRI1 ligand-
161 dependent endocytosis model using BRI1^Q by evaluating the internalization of BRI1^Q-mCit in
162 root meristem epidermal cells (Figure 3A and 3B). The PM pool of BRI1 is regulated by
163 secretion, recycling, and endocytosis. To avoid interference of the newly synthesized and
164 secreted BRI1, we analyzed 5-day-old plants expressing BRI1^Q-mCit treated with 50 μ M of
165 the protein synthesis inhibitor cycloheximide (CHX) for 1.5 h. Interestingly, the PM vs.
166 cytoplasm fluorescence intensity, did not significantly differ between BRI1^Q-mCit and the
167 control BRI1-mCit, both in *bri1* null background (Figures 3A and 3B, upper panel). In
168 addition to the CHX treatment, we applied Brefeldin A (BFA), an inhibitor of endosomal
169 trafficking that is widely used to visualize endocytosis (Geldner et al., 2003). In *Arabidopsis*
170 roots, BFA treatment promotes the formation of BFA bodies, composed of large aggregation
171 of trans-Golgi network/early endosome (TGN/EE) compartments (Geldner et al., 2003; Lam
172 et al., 2009). When combining CHX (50 μ M, 1.5 h) with BFA (50 μ M, 30 min), both BRI1-
173 mCit and BRI1^Q-mCit accumulated in similar size BFA bodies (Figure 3A and 3B, lower
174 panel). These results were in agreement with the measurements of the PM vs. cytoplasm
175 fluorescence intensity in BRI1^Q-mCit (Figure 3A and 3B, upper panel). Comparable PM vs.
176 cytoplasm fluorescence intensity ratios and BFA body size were also obtained when BRI1^Q-
177 mCit was introduced into the Columbia-0 (Col-0) wild type to avoid artefacts in quantitative
178 microscopy due to the strong dwarfism of the *bri1* mutant (Figure 3C and 3D, S2B).

179 Despite the widespread use of CHX and BFA treatments to analyze endocytosis in
180 plant cells, it cannot be excluded that the chemical treatments might cause pleiotropic
181 effects (Oksvold et al., 2012; Smith et al., 2014). To circumvent this problem, we expressed

182 BRI1-mCit and BRI1^Q-mCit under the control of the heat shock-inducible promoter (*pHS*) in
183 the Col-0 background and studied the protein internalization during the recovery phase
184 following induction at 37°C for 1 h. Firstly, we selected transgenic lines expressing
185 *pHS::BRI1-mCit* and *pHS::BRI1^Q-mCit* with similar expression levels following the heat
186 induction (37°C) for 1 h (Figure S2C). Taking advantage of a vertical confocal microscope
187 setup equipped with the TipTracker software (von Wangenheim et al., 2017) that allows the
188 monitoring of growing root tips over time, we observed that BRI1^Q-mCit reached the PM a
189 little later than the BRI1-mCit. However, after a signal intensity peak in the PM, between 87
190 and 99 min, the internalization rate of BRI1-mCit and BRI1^Q-mCit was very similar. Thus,
191 our findings further confirm previous reports (Geldner et al., 2007; Irani et al., 2012;
192 Russinova et al., 2004) that the BRI1 internalization is largely independent of BR binding.
193 After ligand binding and interaction with BAK1, BRI1 is phosphorylated and ubiquitinated,
194 both essential for receptor internalization (Martins et al., 2015; Zhou et al., 2018). However,
195 although BRI1^Q lacked both PTMs, it still had a normal endocytosis. These results reinforce
196 the hypothesis that BRI1 is internalized via more than one endocytic route and probably via
197 different mechanisms. For instance, the BRI1 internalization has been demonstrated to
198 partially depend on both the classical clathrin Adaptor Protein 2 (AP-2) complex that binds to
199 a canonical YXXΦ endocytic motif in BRI1 (Liu et al., 2020) and on ubiquitin recognition
200 machinery, since endocytosis of the ubiquitin-deficient BRI1^{25KR}-mCit or BRI1-mCit in the
201 *pub12 pub13* double mutant was not completely abolished (Martins et al., 2015; Zhou et al.,
202 2018). Similar observations were reported for the borate exporter BOR1, in which AP-2-
203 dependent and AP-2-independent endocytic routes had been activated by low and high borate
204 concentration, respectively (Yoshinari et al., 2019). In mammals, the well-studied epidermal
205 growth factor receptor (EGFR) is also internalized via multiple endocytic routes, including
206 canonical ligand-dependent clathrin-mediated endocytosis and clathrin-independent
207 endocytosis route, which both depend on the ligand concentration (Zhou and Sakurai, 2022),
208 and a ligand-independent route where EGFR endocytosis is induced by stress conditions and
209 does not require kinase activity or ubiquitination (Metz et al., 2021). Taken together, our
210 results show that the BRI1 internalization is not abolished in the BR binding-deficient mutant,
211 similarly to BRI1 YXXΦ endocytic motif mutants (Liu et al., 2020), the BRI1 ubiquitination-
212 deficient mutants (Martins et al., 2015; Zhou et al., 2018) and the BRI1 endocytosis in AP-2
213 mutants (Di Rubbo et al., 2013; Gadeyne et al., 2014). It remains to be established which
214 signals or conditions trigger these different types of BRI1 endocytosis.

215

216 **BRI1^Q can partially complement the xylem phenotype of *bri1***

217 In addition to its primary role in perceiving BRs, recent studies suggest that BRI1 might also
218 have non-canonical functions in sensing cell wall integrity. After disturbance of the cell wall
219 integrity by the inhibition of the pectin de-methyl esterification, BRI1 is recruited together
220 with the RLP44 and BAK1 to activate a BR signaling for a compensatory feedback loop to
221 remodel the cell wall (Wolf et al., 2012). Besides cell wall integrity monitoring, RLP44 is also
222 implicated in controlling xylem cell fate through the phytosulfokine (PSK) signaling
223 (Holzwart et al., 2018). Interestingly, BRI1 and BAK1 are also necessary to regulate the
224 vasculature cell fate, but independently of BRs, because BR biosynthesis mutants have no
225 ectopic xylem in the procambial position present in the *rlp44* and *bri1* mutants (Holzwart et
226 al., 2018, 2020). To test whether BRI1^Q retains its non-BRs receptor functions, we examined
227 if BRI1^Q could still interact with RLP44 (Holzwart et al., 2018). RLP44-RFP was transiently
228 co-expressed with either BRI1-GFP or BRI1^Q-GFP in *Nicotiana benthamiana* leaves and co-
229 immunoprecipitation (Co-IP) assay revealed that RLP44-RFP was co-purified with both BRI1-
230 GFP and BRI1^Q-GFP but not with the negative control, indicating that BRI1^Q, like the wild
231 type BRI1, can form a complex with RLP44 (Figure 4A). Furthermore, confocal analysis of
232 tobacco leaves transiently expressing BRI1-GFP, BRI1^Q-GFP and RLP44-RFP show that both
233 BRI1 and BRI1^Q colocalize with RLP44 in dynamic punctate structures (Figure 4B). The
234 intracellular punctate structures containing RLP44-RFP and BRI1-GFP or BRI1^Q-GFP are
235 probably endosomes, because BRI1 is a *bona fide* endosomal PM cargo (Geldner et al., 2007;
236 Russinova et al., 2004). Moreover, RLP44 had already been shown to localize in endosomal
237 structures in *Arabidopsis* roots (Wolf et al., 2014). Finally, we tested whether BRI1^Q-mCitrin
238 could recover the BR-independent xylem cell fate phenotype of the *bri1* null mutants
239 (Holzwart et al., 2018, 2020). Indeed, BRI1^Q-mCitrin could partially complement the ectopic
240 number of xylem cells present in the *bri1* mutant (Figure 4). Collectively, our result provides
241 evidence that BRI1^Q could still be active in BR-independent pathways.

242 In conclusion, analyses of the crystal structure of the ectodomain of BR receptors and
243 homology modeling allowed us to create a BR binding-deficient BRI1 mutant, BRI1^Q.
244 Characterization of BRI1^Q showed that it displays a clear *bri1*-like phenotype and is unable to
245 respond to exogenous BRs. By means of BRI1^Q as a tool to study BRI1 endocytosis and in
246 agreement with previous observations (Geldner et al., 2007; Irani et al., 2012; Russinova et
247 al., 2004), we conclude that BRI1 internalization can occur without BR binding. Moreover,

248 the BR-binding-deficient BRI1 mutant might provide opportunities to discover additional
249 non-canonical ligand-independent BRI1 functions in vasculature development and other
250 processes (Graeff et al., 2020; Holzwart et al., 2018, 2020).

251

252 **Materials and Methods**

253

254 **Plant materials, growth conditions and treatments.**

255 The experimental model used in this study is Arabidopsis. The wild type used is the
256 *Arabidopsis thaliana* (L.) Heynh. (accession Columbia-0 [Col-0]). For phenotypic analysis,
257 plants were grown in soil in a growth chamber at 22°C, 58% relative humidity, and a 16-h
258 light/8-h dark photoperiod for 6 weeks. The Arabidopsis seeds were surface-sterilized with
259 chlorine gas, and then placed on plates with half-strength Murashige and Skoog medium
260 (½MS) containing 0.5% (w/v) sucrose, 0.8% (w/v) agar, and 2.5 mM methyl ester sulfonate at
261 pH 5.7. After vernalization for 2 days at 4°C, the plates were moved to the growth chamber
262 under a 16-h/8-h light/dark cycle. Wild-type tobacco (*Nicotiana benthamiana*) plants were
263 grown in the greenhouse under a normal 14-h light/10-h dark regime at 25°C. For the
264 microsomal protein preparation, plants were grown for 6 days on plates. For the BRI1
265 internalization assay and the BRI1 transcript analysis, plants were grown for 5 or 7 days on
266 plates. MG-132 (10 mM stock in dimethylsulfoxide [DMSO]), BFA (50 mM stock in DMSO)
267 and CHX (50 mM stock in DMSO) were used at the concentrations indicated in the figure
268 legends.

269

270 **Vector construction and plant transformation.** The BRI1-coding region without the stop
271 codon was cloned into *pMD19-T* (simple) (Takara Biotechnology) to generate *pMD19-BRI1*
272 that was used as a template to generate the mutants BRI1^{Y599F}, BRI1^{M657E},
273 BRI1^{Y597M/Y599F/M657E}, BRI1^{Y597A/Y599A/M657A}, and BRI1^{Y597M/Y599F/Y642A/M657E/F681A} by
274 overlapping PCR and subcloned into *pDONR221* to generate *pDONRP1P2-BRI1* (with
275 mutations). The primers used to generate the BRI1 mutations are listed in Table S1. The
276 destination vectors were generated by recombining *pK7m34GW*, *pB7m34GW*, *pDONRP4P1r-*
277 *pBRI1*, *pDONRP4P1r-pHS* (Marquès-Bueno et al., 2016) *pDONRP4P1r-pBRI1*,
278 *pDONRP4P1r-pHS*, *pDONR221-BRI1*, and *pDONRP2rP3-mCit* (Martins et al., 2015). The
279 resulting constructs were transformed into the heterozygous *bri1* null mutant (GABI_134E10)
280 (Jaillais et al., 2011) or into Col-0 plants by floral dip. For transient expression in tobacco,

281 *pDONR221-BRI1* and *pDONR221-BRI1^Q* were recombined in pK7FWG2 that contained the
282 35S promoter and C-terminal GFP. The Gateway technology (Invitrogen) was used for
283 cloning.

284

285 **Western blot analysis and immunoprecipitation**

286 For the BRI1 expression assay, 5-day-old seedlings were homogenized in liquid nitrogen.
287 Total proteins were extracted with a buffer containing 20 mM Tris-HCl, pH 7.5, 150 mM
288 NaCl, 1% (w/v) sodium dodecyl sulfate (SDS), 100 mM dithiothreitol (DTT), and
289 ethylenediaminetetraacetic acid (EDTA)-free protease inhibitor cocktail cOmplete (Roche).
290 For blocking and antibody dilutions, 3% (w/v) bovine serum albumin (BSA) powder in 0.2%
291 (v/v) Tris-buffered saline-containing Tween-20 was used. For the microsomal fraction
292 isolation, 6-day-old seedlings treated with 50 µM MG-132 for 5 h were ground in liquid
293 nitrogen and resuspended in ice-cold sucrose buffer (100 mM Tris [pH 7.5], 810 mM sucrose,
294 5% [v/v] glycerol, 10 mM EDTA [pH 8.0], 10 mM ethyleneglycoltetraacetic acid [EGTA, pH
295 8.0], 5 mM KCl, protease inhibitor [Sigma-Aldrich], and phosphatase inhibitor [Sigma-
296 Aldrich]). The homogenate was transferred to polyvinyl polypyrrolidone (PVPP) pellets,
297 mixed, and left to rest for 5 min. Samples were centrifuged for 5 min at 600g at 4°C. The
298 supernatant was collected. The extraction was repeated for two more times. The supernatant
299 was filtered through a Miracloth mesh. The same amount of water was added to the clear
300 supernatant and centrifuged at 21,000g for 2 h at 4°C to pellet microsomes (Abas and
301 Luschnig, 2010). The pellet was resuspended in immunoprecipitation buffer (25 mM Tris, pH
302 7.5, 150 mM NaCl, 0.1% [w/v] SDS, protease inhibitor, and phosphatase inhibitor).
303 Immunoprecipitations were carried out on solubilized microsomal proteins with GFP-Trap-
304 MA (Chromotek) according to the manufacturer's protocol. For protein detection, the
305 following antibodies were used: monoclonal α -GFP horseradish peroxidase-coupled (1/5,000;
306 Miltenyi Biotech), monoclonal α -tubulin (1/10,000; Sigma-Aldrich), α -ubiquitin (Ub) P4D1
307 (1/2,500; Millipore), α -pThr (1/2,000; Cell Signaling), α -BES1 (Yin et al., 2002) (1/4,000),
308 and α -BAK1 (1/5,000; custom-made by Eurogentec). For the uncropped blots see Figure S3.

309

310 **Xylem staining**

311 Seven-day-old *Arabidopsis* seedlings were stained with Basic Fuchsin as described (Ursache
312 et al., 2018).

313

314 **Confocal microscopy and image analysis.** For BRI1 localization *Arabidopsis* seedlings were
315 imaged with an Olympus Fluoview1000 confocal laser scanning microscope and a
316 UPLSAPO 60 \times /1.2 n.a. water-corrected immersion objective at digital zoom 2, whereas for
317 BRI1 internalization and BFA treatment, a Leica SP8X confocal microscope was used with a
318 HC PL 584 APO CS2 40x/1.1 n.a. water-corrected immersion objective at digital zoom 5 and
319 3, respectively. The excitation/emission wavelengths were 514 nm/530-600 nm for BRI1-
320 mCitr. For the BRI1 internalization, the membrane of individual cells was selected using the
321 brush tool of ImageJ with a size of 5 pixels as well as using the polygon selection tool to mark
322 the intracellular space. The average intensity of the top 5 % highest pixels for both the PM
323 and the intracellular space was used to obtain a ratio between PM and intracellular
324 fluorescence. The BFA body size was calculated as previously described (Luo et al., 2015).
325 Xylem was imaged with Leica SP8X confocal microscope equipped with a HC PL APO CS2
326 63x/1.20 n.a. water-corrected immersion objective. The excitation/emission wavelengths used
327 were of 561 nm/600-650 nm for Basic Fuchsin staining. The BRI1 heat shock lines were
328 analyzed under a vertical ZEISS LSM900 microscope equipped with a Plan-Apochromat M27
329 20x/ 0.8 n.a. objective. The excitation/emission wavelengths were 514 nm/530-600 nm for
330 BRI1-mCitr. The root tip was tracked over time with the TipTracker software (von
331 Wangenheim et al., 2017). Quantification was obtained by measuring the PM signal of the
332 same cell over time and normalized by the time point with the highest PM signal. Images
333 processing and quantification were performed with the Fiji software package.

334

335 **Grating-coupled interferometry (GCI)**

336 A Creoptix WAVE system (Creoptix AG, Switzerland) was used for the GCI binding assays.
337 Experiments were done on a 4PCH WAVE GCI chip (long polycarboxylate surface; Creoptix
338 AG). After a borate buffer conditioning (100 mM sodium borate, pH 9.0, 1 M NaCl; XanTec
339 Bioanalytics, Düsseldorf, Germany), streptavidin was immobilized through a standard amine
340 coupling protocol, followed by passivation of the surface (0.5% BSA [Roche] in 10 mM
341 sodium acetate, pH 5.0), and final quenching with 1 M ethanolamine, pH 8.0 for 7 min
342 (XanTec Bioanalytics). The LRR ectodomains of wild-type BRI1 and the respective mutants
343 were biotinylated and coupled to the streptavidin-coated chip. For the BL binding
344 experiments, BL was injected in a 1:2 dilution series, starting from 3 μ M, in 20 mM citrate,
345 pH 5.0, 250 mM NaCl at 25°C. Blank injections were used for double referencing and a
346 DMSO calibration curve for bulk correction. All analyses and corrections were done with the

347 Creoptix WAVE control software, with a one-to-one binding model with bulk correction used
348 to fit all experiments.

349

350 **Analytical size-exclusion chromatography (SEC)**

351 Analytical SEC experiments were carried out on a Superdex 200 increase 10/300 GL column
352 (GE Healthcare), preequilibrated in 20 mM sodium citrate, pH 5.0, 250 mM NaCl. 200 µg of
353 protein, injected in a 100-µl volume, was loaded onto the column and elution at 0.75 ml/min
354 was monitored by ultraviolet absorbance at $\lambda = 280$ nm. Peak fractions were analyzed by
355 SDS-PAGE.

356

357 **Right-angle light scattering (RALS).** BRI1 ectodomains (residues 1-788 with a C-terminal
358 Avi-tag as well as a TEV protease cleavable TwinStrep – 9x His tag) were expressed and
359 purified as described previously (Hohmann et al 2018b) and analyzed by size-exclusion
360 chromatography (SEC) paired with a RALS and a refractive index (RI) detector, using an
361 OMNISEC RESOLVE / REVEAL system. The calibration of the instrument was carried out
362 with a BSA standard (Thermo Scientific). In a 50 µl volume, 100 µg of protein was separated
363 on a Superdex 200 increase column (GE Healthcare) in 20 mM sodium citrate, pH 5.0,
364 250 mM NaCl at a column temperature of 35°C and a 0.7 ml/min. Data were analyzed using
365 the OMNISEC software (v10.41).

366

367 **Homology modeling and structure visualization.** BRI^Q ectodomain structure was modeled
368 using the Modeller 9.18 program (Šali and Blundell, 1993) with the BRI1 ectodomain (PDB
369 ID 3RJ0) as a template. The structures of wild type BRI1 and BRI1^Q ectodomains (Figure 1)
370 were visualized by UCSF Chimera (Pettersen et al., 2021). Multiple sequence alignment was
371 prepared using the Jalview program (Waterhouse et al., 2009)

372

373 **RT-qPCR**

374 Seven-day-old seedlings in liquid half-strength Murashige and Skoog medium were
375 transferred to 37°C for 1 h and let to recover at room temperature for another 1 h. Total RNA
376 was extracted with the RNeasy kit (Qiagen). cDNA from RNA was synthesized with the
377 qScript cDNA Supermix (Quantabio). RT-qPCRs were run with SYBR green I Master kit
378 (Roche) on a LightCycler 480 (Roche). The mCitrine expression was normalized to that of
379 ACTIN2 and GAPDH. The cycling conditions were as follows: preincubation at 95°C for

380 10 min; 45 amplification cycles at 95°C for 10 s, 60°C for 15 s, and 72°C for 15 s; melting
381 curve at 95°C for 1 s, and 65°C for 1 s, followed by cooling at 40°C for 10 s.

382

383 **QUANTIFICATION AND STATISTICAL ANALYSIS**

384

385 The data were subjected to statistical analysis using GraphPad Prism
386 (<https://www.graphpad.com/scientific-software/prism/>) and Excel software. Comparisons
387 between groups were made with the Mann Whitney test or two-way ANOVA with subsequent
388 post hoc Sidak's multiple comparisons test. Comparisons between discrete groups were made
389 using Chi-square test. The measurements are shown as box plots displaying the first and third
390 quartiles and split by medians (center lines), with whiskers extending to 1.5-fold the
391 interquartile range from the 25th and 75th percentiles.

392

393 **SUPPLEMENTAL INFORMATION**

394

395 Supplemental Information can be found online

396

397 **ACKNOWLEDGEMENTS**

398

399 We thank Yanhai Yin (Iowa State University, Ames, USA), Gregory Vert (CNRS/Université
400 de Toulouse, France), and Cyril Zipfel (University of Zurich, Switzerland) for providing the
401 anti-BES1 antibody, the *pBRI1:BRI1-mCit/bri1* *Arabidopsis* transgenic line, pDONRP4P1r-
402 pBRI1, pDONRP1P2-BRI1 and pDONRP2rP3-mCit plasmids, and information for making
403 the anti-BAK1 antibody, respectively, and Martine De Cock for help in preparing the
404 manuscript. This work was supported by Ghent University Special Research Fund Grant
405 (BOF15/24J/048 to E.R.), the Research Foundation-Flanders (project G022516N to E.R. and
406 a postdoctoral fellowship 12R7819N to N.V.), the European Research Council (ERC Co T-
407 Rex grant 682436 to D.V.D), the Swiss National Science Foundation (project number
408 31003A_176237, to M.H.), the Howard Hughes Medical Institute (to M.H.) and the German
409 Research Foundation (DFG) (project WO 1660/6-2 to S.W.).

410

411 **AUTHOR CONTRIBUTIONS**

412

413 L.A.N.C., D.L., N.V., and E.R. conceived, designed, and performed the research. R.P. did
414 modeling. J. L., G.W., and Y.J. contributed unpublished materials. U.H., and M.H. did
415 binding experiments. L.A.N.C., A.S. and S.W. did the xylem phenotype experiments. D.V.D.
416 helped with data analysis and manuscript finalization. L.A.N.C., D.L., and E.R. wrote the
417 manuscript. All authors commented on the results and on the manuscript text.

418

419 DECLARATION OF INTERESTS

420

421 **The authors declare no competing interests.**

422

423 REFERENCES

424

425 Abas, L., and Luschnig, C. (2010). Maximum yields of microsomal-type membranes from
426 small amounts of plant material without requiring ultracentrifugation. *Anal. Biochem.*
427 *401*, 217-227.

428 Asami, T., Min, Y.K., Nagata, N., Yamagishi, K., Takatsuto, S., Fujioka, S., Murofushi, N.,
429 Yamaguchi, I., and Yoshida, S. (2000). Characterization of brassinazole, a triazole-type
430 brassinosteroid biosynthesis inhibitor. *Plant Physiol.* *123*, 93-100.

431 Belkhadir, Y., and Jaillais, Y. (2015). The molecular circuitry of brassinosteroid signaling.
432 *New Phytol.* *206*, 522-540.

433 Caño-Delgado, A., Yin, Y., Yu, C., Vafeados, D., Mora-García, S., Cheng, J.-C., Nam, K.H.,
434 Li, J., and Chory, J. (2004). BRL1 and BRL3 are novel brassinosteroid receptors that
435 function in vascular differentiation in *Arabidopsis*. *Development* *131*, 5341-5351.

436 Chen, L.-G., Gao, Z., Zhao, Z., Liu, X., Li, Y., Zhang, Y., Liu, X., Sun, Y., and Tang, W.
437 (2019). BZR1 Family Transcription Factors Function Redundantly and Indispensably in
438 BR Signaling but Exhibit BRI1-Independent Function in Regulating Anther
439 Development in *Arabidopsis*. *Mol. Plant* *12*, 1408–1415.

440 Di Rubbo, S., Irani, N.G., Kim, S.Y., Xu, Z.-Y., Gadeyne, A., Dejonghe, W., Vanhoutte, I.,
441 Persiau, G., Eeckhout, D., Simon, S., et al. (2013). The clathrin adaptor complex AP-2
442 mediates endocytosis of BRASSINOSTEROID INSENSITIVE1 in *Arabidopsis*. *Plant*
443 *Cell* *25*, 2986-2997.

444 Geldner, N., Anders, N., Wolters, H., Keicher, J., Kornberger, W., Muller, P., Delbarre, A.,
445 Ueda, T., Nakano, A., and Jürgens, G. (2003). The *Arabidopsis* GNOM ARF-GEF

446 mediates endosomal recycling, auxin transport, and auxin-dependent plant growth. *Cell*
447 112, 219-230.

448 Geldner, N., Hyman, D.L., Wang, X., Schumacher, K., and Chory, J. (2007). Endosomal
449 signaling of plant steroid receptor kinase BRI1. *Genes Dev.* 21, 1598-1602.

450 Graeff, M., Rana, S., Marhava, P., Moret, B., and Hardtke, C.S. (2020). Local and Systemic
451 Effects of Brassinosteroid Perception in Developing Phloem. *Curr. Biol.* 30, 1626-
452 1638.e3.

453 He, Z., Wang, Z.-Y., Li, J., Zhu, Q., Lamb, C., Ronald, P., and Chory, J. (2000). Perception of
454 brassinosteroids by the extracellular domain of the receptor kinase BRI1. *Science* 288,
455 2360-2363.

456 Hohmann, U., Nicolet, J., Moretti, A., Hothorn, L.A., and Hothorn, M. (2018a). The SERK3
457 *elongated* allele defines a role for BIR ectodomains in brassinosteroid signalling. *Nat.*
458 *Plants* 4, 345-351.

459 Hohmann, U., Santiago, J., Nicolet, J., Olsson, V., Spiga, F.M., Hothorn, L.A., Butenko,
460 M.A., and Hothorn, M. (2018b). Mechanistic basis for the activation of plant membrane
461 receptor kinases by SERK-family coreceptors. *Proc. Natl. Acad. Sci. USA* 115, 3488-
462 3493.

463 Holzwart, E., Huerta, A.I., Glöckner, N., Garnelo Gómez, B., Wanke, F., Augustin, S.,
464 Askani, J.C., Schürholz, A.-K., Harter, K., and Wolf, S. (2018). BRI1 controls vascular
465 cell fate in the *Arabidopsis* root through RLP44 and phytosulfokine signaling. *Proc.*
466 *Natl. Acad. Sci. USA* 115, 11838-11843.

467 Holzwart, E., Wanke, F., Glöckner, N., Höfte, H., Harter, K., and Wolf, S. (2020). A mutant
468 allele uncouples the brassinosteroid-dependent and independent functions of
469 BRASSINOSTEROID INSENSITIVE 1. *Plant Physiol.* 182, 669-678.

470 Hothorn, M., Belkhadir, Y., Dreux, M., Dabi, T., Noel, J.P., Wilson, I.A., and Chory, J.
471 (2011). Structural basis of steroid hormone perception by the receptor kinase BRI1.
472 *Nature* 474, 467-471.

473 Irani, N.G., Di Rubbo, S., Mytte, E., Van den Begin, J., Schneider-Pizón, J., Hniliková, J.,
474 Šišá, M., Buyst, D., Vilarrasa-Blasi, J., Szatmári, A.-M., et al. (2012). Fluorescent
475 castasterone reveals BRI1 signaling from the plasma membrane. *Nat. Chem. Biol.* 8,
476 583-589.

477 Jaillais, Y., Belkadir, Y., Balsemão-Pires, E., Dangl, J.L., and Chory, J. (2011). Extracellular
478 leucine-rich repeats as a platform for receptor/coreceptor complex formation. *Proc.*
479 *Natl. Acad. Sci. USA* *108*, 8503-8507.

480 Kinoshita, T., Caño-Delgado, A., Seto, H., Hiranuma, S., Fujioka, S., Yoshida, S., and Chory,
481 J. (2005). Binding of brassinosteroids to the extracellular domain of plant receptor
482 kinase BRI1. *Nature* *433*, 167-171.

483 Lam, S.K., Cai, Y., Tse, Y.C., Wang, J., Law, A.H.Y., Pimpl, P., Chan, H.Y.E., Xia, J., and
484 Jiang, L. (2009). BFA-induced compartments from the Golgi apparatus and *trans*-Golgi
485 network/early endosome are distinct in plant cells. *Plant J.* *60*, 865-881.

486 Li, J., Wen, J., Lease, K.A., Doke, J.T., Tax, F.E., and Walker, J.C. (2002). BAK1, an
487 *Arabidopsis* LRR receptor-like protein kinase, interacts with BRI1 and modulates
488 brassinosteroid signaling. *Cell* *110*, 213-222.

489 Liu, D., Kumar, R., Claus, L.A.N., Johnson, A.J., Siao, W., Vanhoutte, I., Wang, P., Bender,
490 K.W., Yperman, K., Martins, S., et al. (2020). Endocytosis of BRASSINOSTEROID
491 INSENSITIVE1 is partly driven by a canonical Tyr-based motif. *Plant Cell* *32*, 3598-
492 3612.

493 Luo, Y., Scholl, S., Doering, A., Zhang, Y., Irani, N.G., Rubbo, S.D., Neumetzler, L.,
494 Krishnamoorthy, P., Van Houtte, I., Mynne, E., et al. (2015). V-ATPase activity in the
495 TGN/EE is required for exocytosis and recycling in *Arabidopsis*. *Nat. Plants* *1*, 15094.

496 Luo, Y., Takagi, J., Claus, L.A.N., Zhang, C., Yasuda, S., Hasegawa, Y., Yamaguchi, J.,
497 Shan, L., Russinova, E., and Sato, T. (2022). Deubiquitinating enzymes UBP12 and
498 UBP13 stabilize the brassinosteroid receptor BRI1. *EMBO Rep.* *23*, e53354.

499 Martins, S., Dohmann, E.M.N., Cayrel, A., Johnson, A., Fischer, W., Pojer, F., Satiat-
500 Jeunemaître, B., Jaillais, Y., Chory, J., Geldner, N., and Vert, G. (2015). Internalization
501 and vacuolar targeting of the brassinosteroid hormone receptor BRI1 are regulated by
502 ubiquitination. *Nat. Commun.* *6*, 6151.

503 Metz, C., Oyanadel, C., Jung, J., Retamal, C., Cancino, J., Barra, J., Venegas, J., Du, G., Soza,
504 A., and González, A. (2021). Phosphatidic acid-PKA signaling regulates p38 and
505 ERK1/2 functions in ligand-independent EGFR endocytosis. *Traffic* *22*, 345-361.

506 Noguchi, T., Fujioka, S., Choe, S., Takatsuto, S., Yoshida, S., Yuan, H., Feldmann, K.A., and
507 Tax, F.E. (1999). Brassinosteroid-insensitive dwarf mutants of *Arabidopsis* accumulate
508 brassinosteroids. *Plant Physiol.* *121*, 743-752.

509 Nolan, T.M., Vukašinović, N., Liu, D., Russinova, E., and Yin, Y. (2020). Brassinosteroids:
510 multidimensional regulators of plant growth, development, and stress responses. *Plant*
511 *Cell* 32, 295-318.

512 Oksvold, M.P., Pedersen, N.M., Forfang, L., and Smeland, E.B. (2012). Effect of
513 cycloheximide on epidermal growth factor receptor trafficking and signaling. *FEBS*
514 *Lett.* 586, 3575-3581.

515 Pettersen, E.F., Goddard, T.D., Huang, C.C., Meng, E.C., Couch, G.S., Croll, T.I., Morris,
516 J.H., and Ferrin, T.E. (2021). UCSF ChimeraX: Structure visualization for researchers,
517 educators, and developers. *Protein Sci.* 30, 70-82.

518 Russinova, E., Borst, J.-W., Kwaaitaal, M., Caño-Delgado, A., Yin, Y., Chory, J., and de
519 Vries, S.C. (2004). Heterodimerization and endocytosis of *Arabidopsis* brassinosteroid
520 receptors BRI1 and AtSERK3 (BAK1). *Plant Cell* 16, 3216-3229.

521 Šali, A. and Blundell, T.L. (1993). Comparative protein modelling by satisfaction of spatial
522 restraints. *J. Mol. Biol.* 234, 779-815.

523 She, J., Han, Z., Kim, T.-W., Wang, J., Cheng, W., Chang, J., Shi, S., Wang, J., Yang, M.,
524 Wang, Z.-Y., and Chai, J. (2011). Structural insight into brassinosteroid perception by
525 BRI1. *Nature* 474, 472-476.

526 Smith, J.M., Salamango, D.J., Leslie, M.E., Collins, C.A., and Heese, A. (2014). Sensitivity to
527 Flg22 is modulated by ligand-induced degradation and de novo synthesis of the
528 endogenous flagellin-receptor FLAGELLIN-SENSING2. *Plant Physiol.* 164, 440-454.

529 Ursache, R., Andersen, T.G., Marhavý, P., and Geldner, N. (2018). A protocol for combining
530 fluorescent proteins with histological stains for diverse cell wall components. *Plant J.*
531 93, 399-412.

532 von Wangenheim, D., Hauschild, R., Fendrych, M., Barone, V., Benková, E., and Friml, J.
533 (2017). Live tracking of moving samples in confocal microscopy for vertically grown
534 roots. *eLife* 6, e26792.

535 Wang, X., and Chory, J. (2006). Brassinosteroids regulate dissociation of BKI1, a negative
536 regulator of BRI1 signaling, from the plasma membrane. *Science* 313, 1118-1122.

537 Wang, Z.-Y., Nakano, T., Gendron, J., He, J., Chen, M., Vafeados, D., Yang, Y., Fujioka, S.,
538 Yoshida, S., Asami, T., and Chory, J. (2002). Nuclear-localized BZR1 mediates
539 brassinosteroid-induced growth and feedback suppression of brassinosteroid
540 biosynthesis. *Dev. Cell* 2, 505-513.

541 Wang, Z.-Y., Seto, H., Fujioka, S., Yoshida, S., and Chory, J. (2001). BRI1 is a critical
542 component of a plasma-membrane receptor for plant steroids. *Nature* *410*, 380-383.

543 Waterhouse, A.M., Procter, J.B., Martin, D.M.A., Clamp, M., and Barton, G.J. (2009).
544 Jalview Version 2-A multiple sequence alignment editor and analysis workbench.
545 *Bioinformatics* *25*, 1189–1191.

546 Wolf, S., Mravec, J., Greiner, S., Mouille, G., and Höfte, H. (2012). Plant cell wall
547 homeostasis is mediated by brassinosteroid feedback signaling. *Curr. Biol.* *22*, 1732-
548 1737.

549 Wolf, S., van der Does, D., Ladwig, F., Sticht, C., Kolbeck, A., Schürholz, A.-K., Augustin,
550 S., Keinath, N., Rausch, T., Greiner, S., et al. (2014). A receptor-like protein mediates
551 the response to pectin modification by activating brassinosteroid signaling. *Proc. Natl.*
552 *Acad. Sci. USA* *111*, 15261-15266.

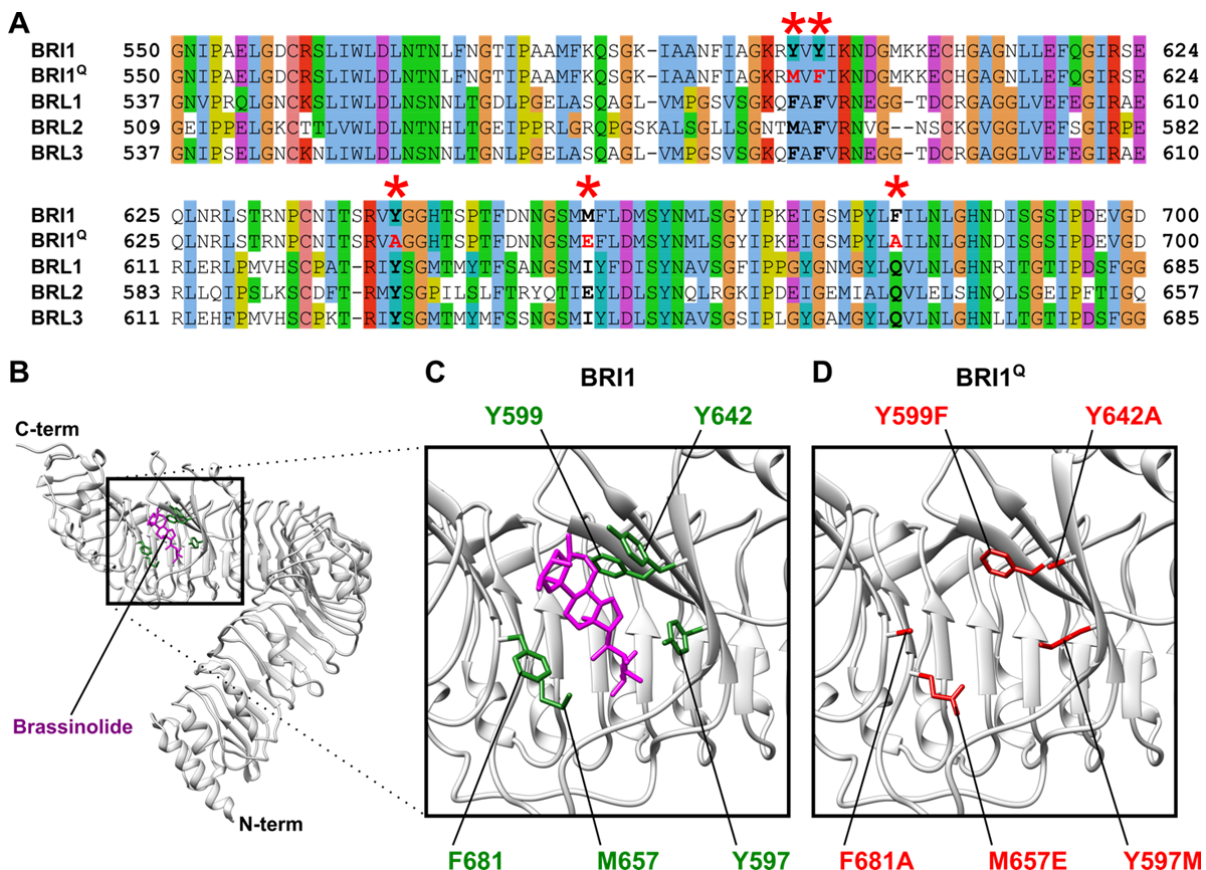
553 Yin, Y., Wang, Z.-Y., Mora-Garcia, S., Li, J., Yoshida, S., Asami, T., and Chory, J. (2002).
554 BES1 accumulates in the nucleus in response to brassinosteroids to regulate gene
555 expression and promote stem elongation. *Cell* *109*, 181-191.

556 Yoshinari, A., Hosokawa, T., Amano, T., Beier, M.P., Kunieda, T., Shimada, T., Hara-
557 Nishimura, I., Naito, S., and Takano, J. (2019). Polar localization of the borate exporter
558 BOR1 requires AP2-dependent endocytosis. *Plant Physiol.* *179*, 1569-1580.

559 Zhou, J., Liu, D., Wang, P., Ma, X., Lin, W., Chen, S., Mishev, K., Lu, D., Kumar, R.,
560 Vanhoutte, I., et al. (2018). Regulation of *Arabidopsis* brassinosteroid receptor BRI1
561 endocytosis and degradation by plant U-box PUB12/PUB13-mediated ubiquitination.
562 *Proc. Natl. Acad. Sci. USA* *115*, E1906-E1915.

563 Zhou, Y., and Sakurai, H. (2022). New trend in ligand-induced EGFR trafficking: a dual-
564 mode clathrin-mediated endocytosis model. *J. Proteomics* *255*, 104503.

565



566 **Figure 1. Selection of the essential residues for BR binding in the BRI1 ectodomain.**

567

568 (A) Sequence alignment of the wild type BRI1 ectodomain (only the region corresponding to

569 BRI1 550-700 is shown) with that of BRL1, BRL2 and BRL3 and BRI1^Q with the mutated

570 residues highlighted in red. The mutated residues are marked with an asterisk.

571

572 (B) The BRI1 ectodomain structure in a complex with brassinolide (BL) (Protein Data Bank

573 ID 3RJ0).

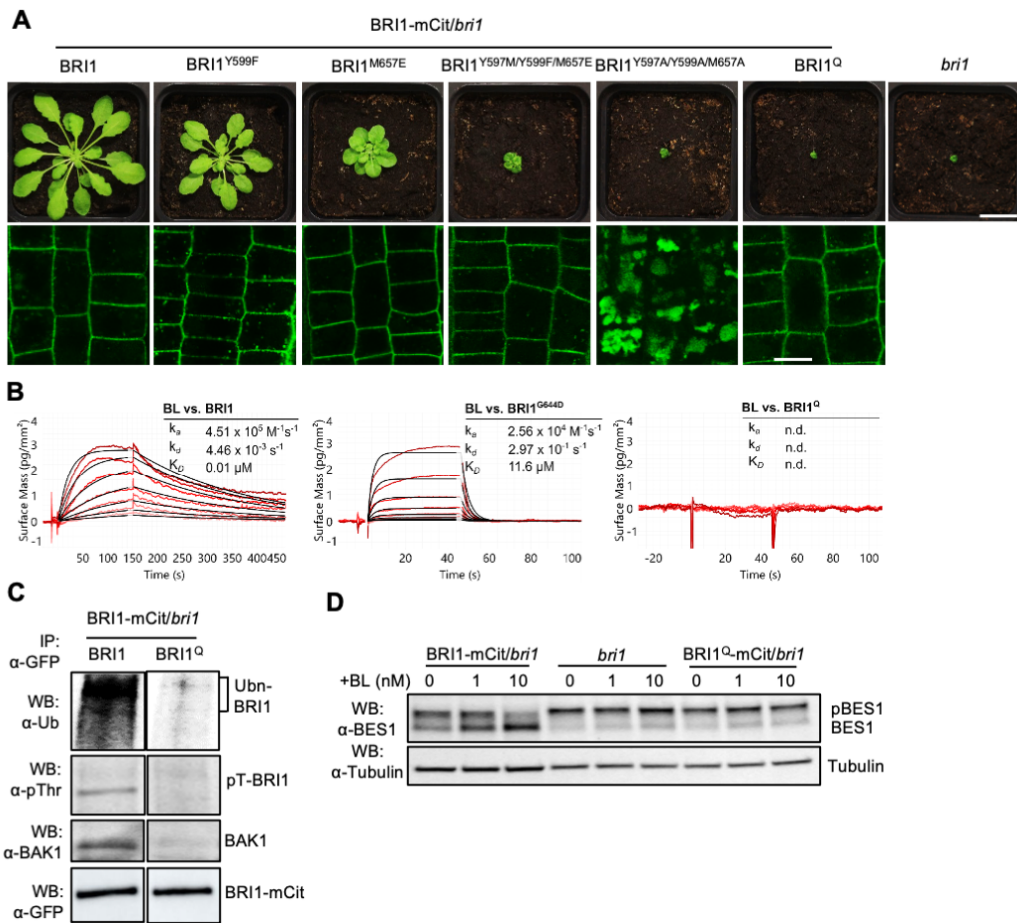
574 (C and D) The five residues selected are indicated as single-letter abbreviation with their

575 locations, either colored in green for wild type BRI1 or in red for BRI1^Q. The figures (B-D)

576 were generated with UCSF Chimera where the BL molecule is shown in a balls-and-sticks

577 representation and colored in purple.

578



579
580

581 **Figure 2. BRI1^Q cannot bind BL.**

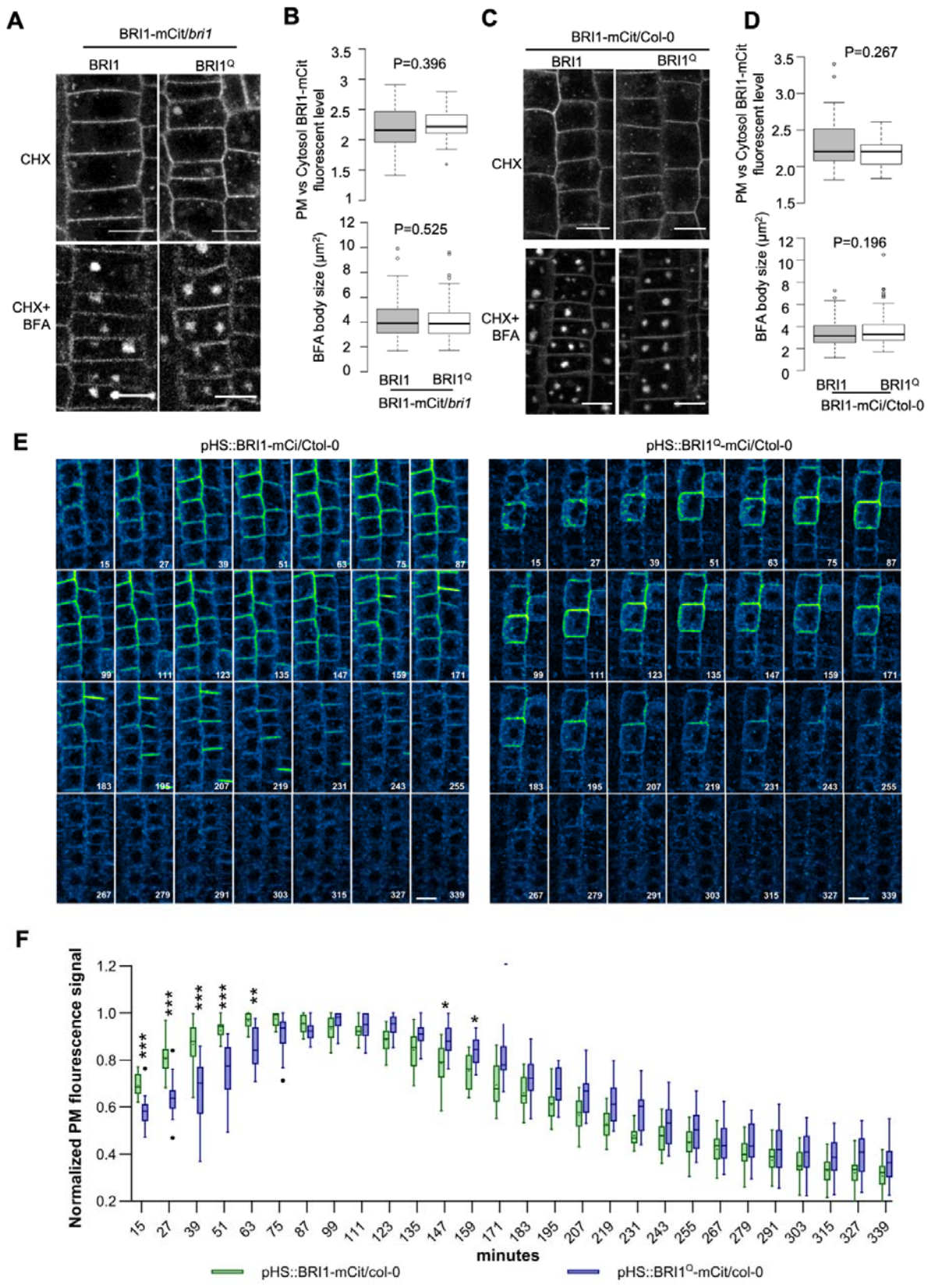
582 (A) Phenotypes (upper panel) and subcellular localizations (lower panel) of homozygous *bri1*
583 mutant transgenic plants expressing the indicated BRI1 isoform mutations grown in short-day
584 cycle for 6 weeks. The quintuple BRI1^{Y597M/Y599F/Y642A/M657E/F681A} mutation is designated
585 BRI1^Q. Epidermal root meristem cells of 5-day-old seedlings were imaged. Scale bars, 2 cm
586 (upper panel) and 10 μm (lower panel).

587 (B) Binding kinetics for BL vs wild-type BRI1, BRI1^{G644D} and BRI1^Q as obtained from
588 grating-coupled interferometry (GCI). Sensograms with recorded data are shown in red with
589 the respective fits in black (when applicable) and include the corresponding association rate
590 constant (k_a), dissociation rate constant (k_d) and dissociation constant (K_D).

591 (C) BRI1-mCitrin and BRI1^Q-mCitrin phosphorylation and ubiquitination state and interaction with
592 BAK1 were tested by isolation of microsomal fractions of 5-day-old seedlings followed by
593 immunoprecipitation (IP) and Western blot (WB) analysis with α-ubiquitin (α-Ub), α-
594 pThreonine (α-pThr) and α-BAK1 antibodies.

595 (D) BES1 phosphorylation state assessed in 5-day-old seedlings treated with DMSO, 1 nM or
596 10 nM BL for 1 h were subjected to WB analysis with the α -BES1 antibody; α -tubulin was
597 used as loading control.

598



599

600

601 **Figure 3. BRI1^Q endocytosis is independent of ligand binding.**

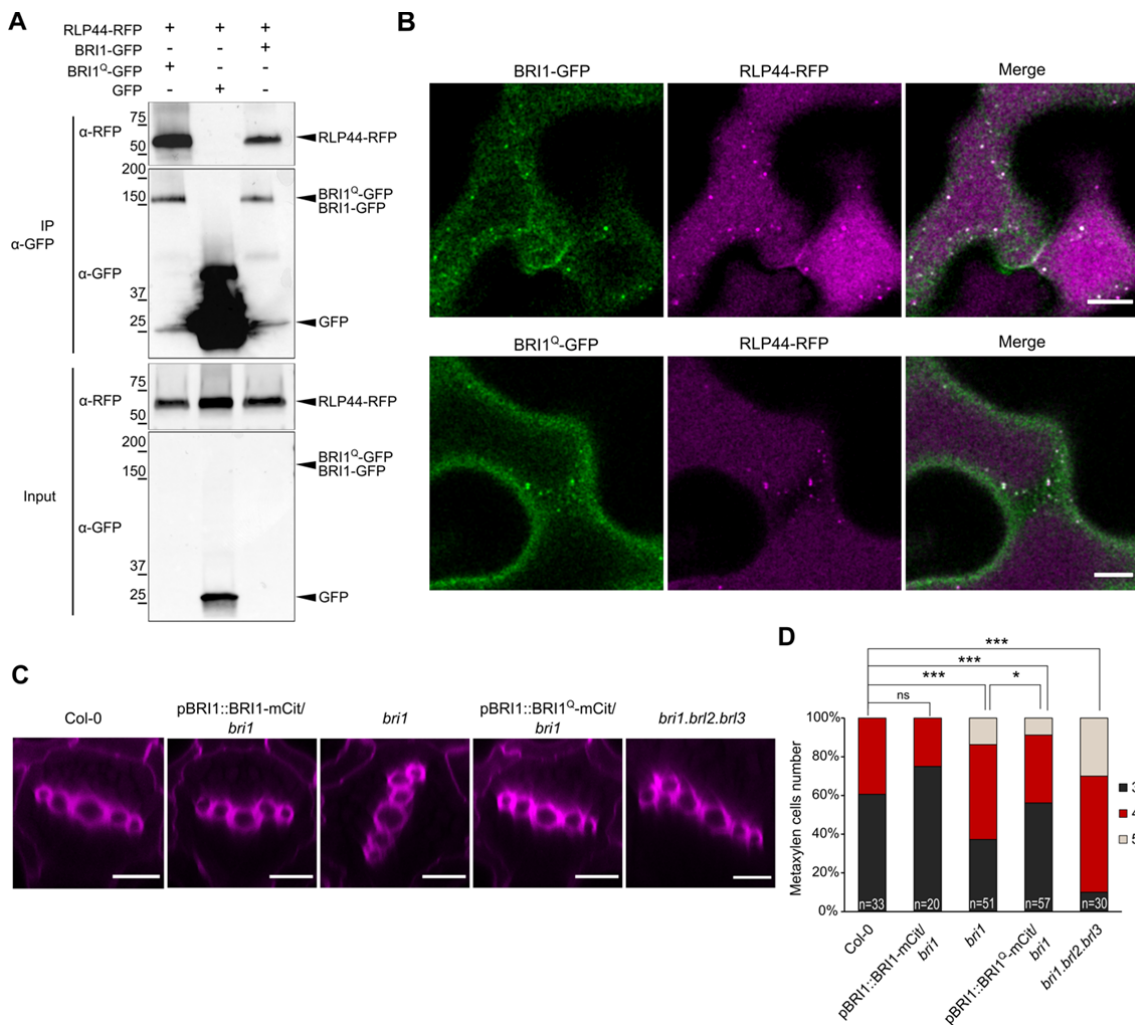
602 (A and C) Representative confocal images of epidermal root meristem cells of 5-day-old
603 seedlings expressing BRI1-mCitrine or BRI1^Q-mCitrine treated with CHX (50 μ M) for 1.5 h or
604 pretreated with CHX for 1 h, followed by treatment for 30 min with CHX and BFA (50 μ M).

605 Scale bar, 10 μ m.

606 (B and D) Plasma membrane (PM) *vs* cytosol BRI1-mCitrine fluorescence and BFA body
607 size. For each line, 15 cells from at least 5 seedlings were measured. Statistical analysis was
608 performed using Mann Whitney test.

609 (E and F) Time series analysis of meristem epidermal cells of 5-day-old seedling expressing
610 BRI1-mCitrine or BRI1^Q-mCitrine after heat induction (1 h at 37°C). Images were taken with a
611 vertical confocal microscope with a 12 min interval between the frames. Scale bar, 10 μ m.
612 Plasma membrane signal intensity of the same cells was quantified for all time points and the
613 signal peak was set as 1. Four roots and 3 to 5 cells were measured per genotype. Asterisks
614 indicate statistically significant differences, * $P<0.05$, ** $P<0.01$, *** $P<0.001$, Two-way
615 ANOVA post hoc Sidak's multiple comparisons test.

616



617

618 **Figure 4. BRI1^Q partially recover *bri1* xylem cell fate phenotype.**

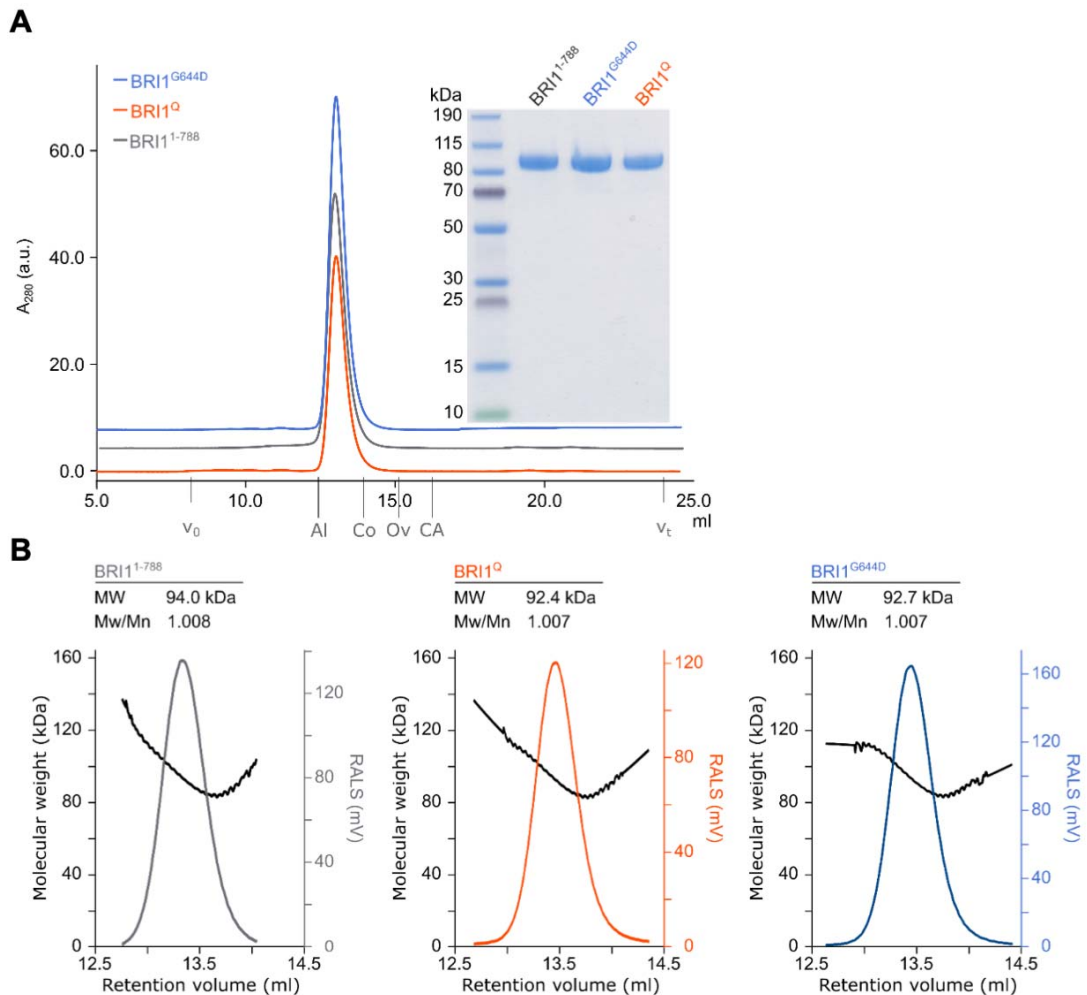
619 (A) Coimmunoprecipitation of RLP44-RFP transiently co-expressed with BRI1-GFP, BRI1^Q-
620 GFP, or free GFP (negative control) in *Nicotiana benthamiana* leaf epidermal cells. Proteins
621 were extracted (Input) and immunoprecipitated (IP) by means of magnetic GFP beads. The
622 immunoblot was done with α-GFP and α-RFP antibodies.

623 (B) Co-localization of RLP44-RFP with BRI1-GFP or BRI1^Q-GFP in subcortical discrete
624 punctate structures in *Nicotiana benthamiana* leaf epidermal cells. Scale bar, 10 μm.

625 (C) 7-day-old roots stained with Basic Fuchsin for the visualization of xylem cells. Scale bar,
626 10 μm.

627 (D) Frequency quantification of roots with the indicated number of metaxylem cells. Asterisks
628 indicate statistically significant differences, * $P<0.05$, ** $P<0.01$, *** $P<0.001$, Chi-square
629 test. $n=20-57$ as indicated.

630

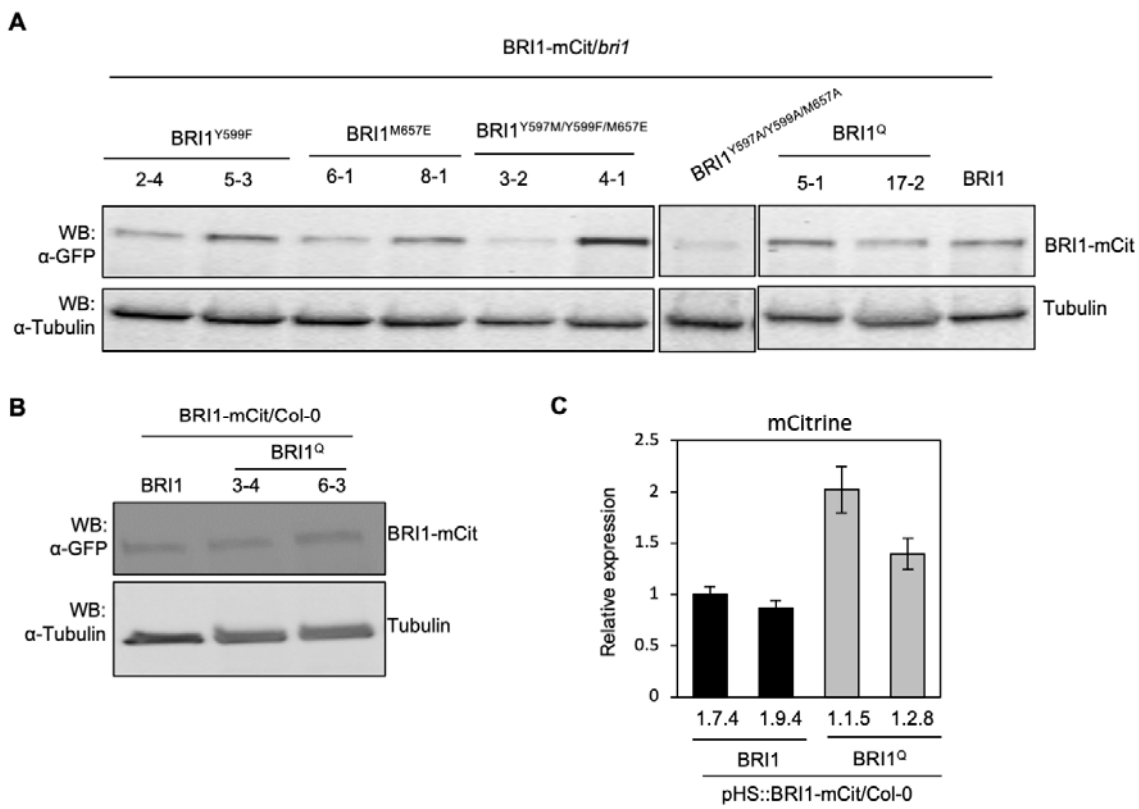


632 **Figure S1. Purity and oligomeric state of wild-type and mutant BRI1 ectodomains.**

633 (A) Analytical size exclusion chromatography traces of BRI1¹⁻⁷⁸⁸ (grey), BRI1^{G644D} (blue) and
634 BRI1^Q (orange) with the SDS-PAGE analysis of pooled peak fractions alongside. Indicated
635 are the void volume (v_0), the total column volume (v_t) and the elution volumes for molecular
636 mass standards (aldolase [Al], 158 kDa; conalbumin [Co], 75 kDa; ovalbumin [Ov], 43 kDa;
637 and carbonic anhydrase [Ca], 29 kDa). Coomassie-stained SDS-PAGE containing 5 μ g of the
638 indicated wild-type or mutated BRI1 ectodomains were isolated from monomeric peak
639 fractions purified by size-exclusion chromatography.

640 (B) Analysis of the oligomeric state of BRI1 ectodomains. Shown are raw right-angle light
641 scattering traces (grey, blue, and orange) and extrapolated molecular weight (black) of BRI1¹⁻
642 ⁷⁸⁸, BRI1^Q, and BRI1^{G644D}, including observed molecular weight (MW) and the dispersity

643 (Mw/Mn). The theoretical molecular weight is 83.5 kDa for BRI1¹⁻⁷⁸⁸, 83.3 kDa for BRI1^Q
644 and 83.6 kDa for BRI1^{G644D}.



645

646 **Figure S2. BRI1 expression in different BRI1 transgenic lines.**

647 (A and B) Total proteins isolated from 5-day-old seedlings and detected by Western blot (WB)
648 with α -GFP antibodies to detect the BRI1-mCitrine (mCitrine). Numbers indicate individual lines.
649 α -tubulin antibodies were used to show equilibrate protein loading.

650 (C) Real-time quantitative reverse transcription PCR (qRT-PCR) analysis of mCitrine. Total
651 RNA was isolated from 7-day-old seedlings of two independent transgenic lines. The
652 seedlings in liquid half-strength Murashige and Skoog medium were transferred to 37°C for h
653 and left to recover at room temperature for 1 h. *GAPDH* and *ACTIN2* were used as
654 normalization controls. In the graph, the mean \pm SD ($n=3$) is presented.

655

Figure 2C

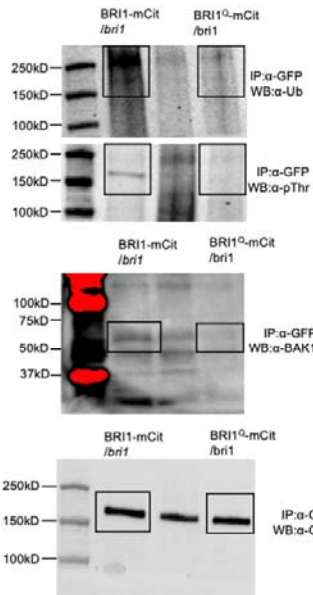


Figure 4A

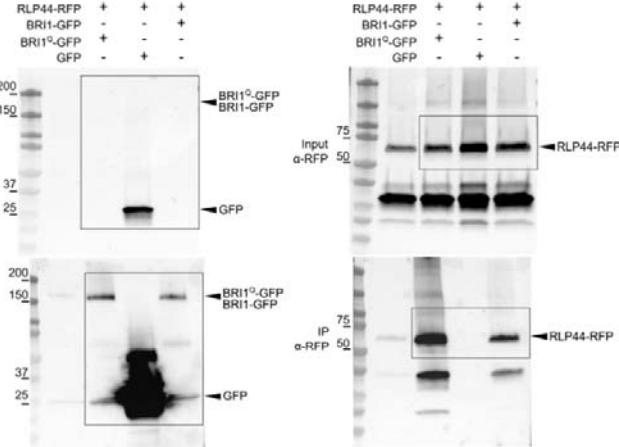


Figure 2D

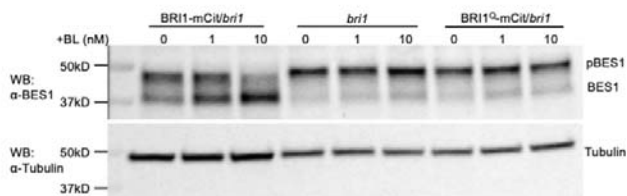


Figure S1B

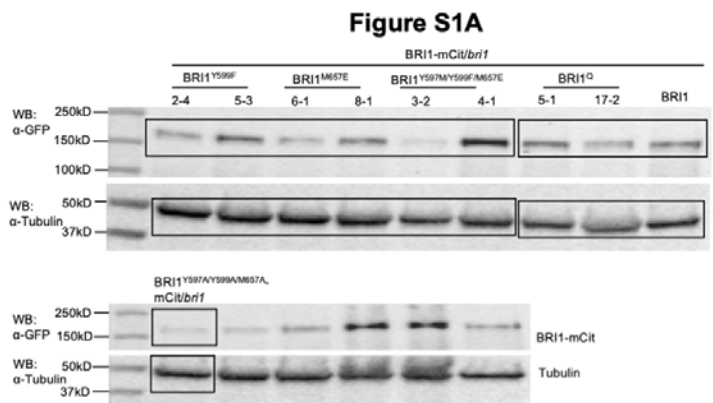
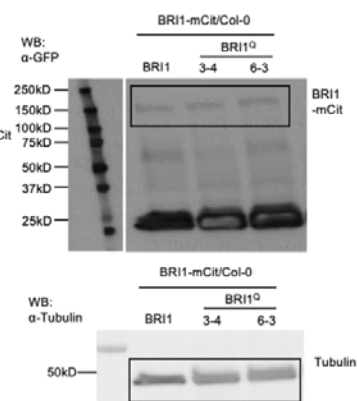


Figure S1A



656

657 **Figure S3. Source blots.**
658

659 **Table S1. List of oligonucleotides used in this study**

Primer Name	Sequence (5'-3')	Description
BRI1_Y599F_FW	GAGGTACTTTTATCAAAACGATG	Generate Y599F mutation in BRI1
BRI1_Y599F_RV	CATCGTTTGATAAAAACGTACCTC	
BRI1_Y597M/Y599F_FW	GCCGTAAGAGGATGGTTTATCAAAACGATG	Generate Y597M/Y599F mutation in BRI1
BRI1_Y597M/Y599F_RV	CATCGTTTGATAAAAACCATCCTTACCGGC	
BRI1_M657E_FW	CAATGGTTGATGGAGTTCTGGACATG	Generate M657E mutation in BRI1
BRI1_M657E_RV	CATGCCAGAAACTCCATCGAACCATG	
BRI1_Y597A/Y599A_FW	GCCGTAAGAGGGCCGTTGCTATCAAAACGATG	Generate Y597A/Y599A mutation in BRI1
BRI1_Y597A/Y599A_RV	CATCGTTTGATAGCAACGGCCCTTACCGGC	
BRI1_Y642A_FW	CACTAGCAGAGTCGCTGGAGGTACACTTC	Generate Y642A mutation in BRI1
BRI1_Y642A_RV	GAAGTGTGACCTCCAGCGACTCTGCTAGTG	
BRI1_M657A_FW	CAATGGTTGATGGCGTTCTGGACATG	Generate M657A mutation in BRI1
BRI1_M657A_RV	CATGCCAGAAACGCCATCGAACCATG	
BRI1_F681A_FW	GATGCCATTCTGGCTATTCTCAATTGG	Generate F681A mutation in BRI1
BRI1_F681A_RV	CCAAATTGAGAATAGCCAGATAAGGCATC	
BRI1_FW	CCGTGTACTTCGATGGCGTTA	qRT-PCR
BRI1_RV	GAGAGACAGGAGAGACGGAGGAC	
Actin2_FW	GATGAGGCAGGTCCAGGAATC	
Actin2_RV	AACCCCAGCTTTAAGCCTTT	
mCit_FW	AGGACGACGGCAACTACAAG	
mCit_RV	TTCTGTTGCGGCCATGAT	
GAPDH_FW	TTGGTGACAAACAGGTCAAGCA	Genotyping <i>bri1</i>
GAPDH_RV	AAACTTGTGCTCAATGCAATC	
BRI1_deletion	CAATTCTCCGGGAACATTCC	
BRI1_3'UTR	CTGACCCCTAGATGATTTGATGTT	
BRI1F_1	CTCAAAGTACTTGATCTG	
Gabi-T-DNA	ATATTGACCATCATACTCATTGC	

660

Parsed Citations

Abas, L., and Luschnig, C. (2010). Maximum yields of microsomal-type membranes from small amounts of plant material without requiring ultracentrifugation. *Anal. Biochem.* 401, 217-227.

Google Scholar: [Author Only](#) [Title Only](#) [Author and Title](#)

Asami, T., Min, Y.K., Nagata, N., Yamagishi, K., Takatsuto, S., Fujioka, S., Murofushi, N., Yamaguchi, I., and Yoshida, S. (2000). Characterization of brassinazole, a triazole-type brassinosteroid biosynthesis inhibitor. *Plant Physiol.* 123, 93-100.

Google Scholar: [Author Only](#) [Title Only](#) [Author and Title](#)

Belkhadir, Y., and Jaillais, Y. (2015). The molecular circuitry of brassinosteroid signaling. *New Phytol.* 206, 522-540.

Google Scholar: [Author Only](#) [Title Only](#) [Author and Title](#)

Caño-Delgado, A., Yin, Y., Yu, C., Vafeados, D., Mora-García, S., Cheng, J.-C., Nam, K.H., Li, J., and Chory, J. (2004). BRL1 and BRL3 are novel brassinosteroid receptors that function in vascular differentiation in *Arabidopsis*. *Development* 131, 5341-5351.

Google Scholar: [Author Only](#) [Title Only](#) [Author and Title](#)

Chen, L.-G., Gao, Z., Zhao, Z., Liu, X., Li, Y., Zhang, Y., Liu, X., Sun, Y., and Tang, W. (2019). BZR1 Family Transcription Factors Function Redundantly and Indispensably in BR Signaling but Exhibit BRI1-Independent Function in Regulating Anther Development in *Arabidopsis*. *Mol. Plant* 12, 1408-1415.

Google Scholar: [Author Only](#) [Title Only](#) [Author and Title](#)

Di Rubbo, S., Irani, N.G., Kim, S.Y., Xu, Z-Y., Gadeyne, A., Dejonghe, W., Vanhoutte, I., Persiau, G., Eeckhout, D., Simon, S., et al. (2013). The clathrin adaptor complex AP-2 mediates endocytosis of BRASSINOSTEROID INSENSITIVE1 in *Arabidopsis*. *Plant Cell* 25, 2986-2997.

Google Scholar: [Author Only](#) [Title Only](#) [Author and Title](#)

Geldner, N., Anders, N., Wolters, H., Keicher, J., Kornberger, W., Muller, P., Delbarre, A., Ueda, T., Nakano, A., and Jürgens, G. (2003). The *Arabidopsis* GNOM ARF-GEF mediates endosomal recycling, auxin transport, and auxin-dependent plant growth. *Cell* 112, 219-230.

Google Scholar: [Author Only](#) [Title Only](#) [Author and Title](#)

Geldner, N., Hyman, D.L., Wang, X., Schumacher, K., and Chory, J. (2007). Endosomal signaling of plant steroid receptor kinase BRI1. *Genes Dev.* 21, 1598-1602.

Google Scholar: [Author Only](#) [Title Only](#) [Author and Title](#)

Graeff, M., Rana, S., Marhava, P., Moret, B., and Hardtke, C.S. (2020). Local and Systemic Effects of Brassinosteroid Perception in Developing Phloem. *Curr. Biol.* 30, 1626-1638.e3.

Google Scholar: [Author Only](#) [Title Only](#) [Author and Title](#)

He, Z., Wang, Z-Y., Li, J., Zhu, Q., Lamb, C., Ronald, P., and Chory, J. (2000). Perception of brassinosteroids by the extracellular domain of the receptor kinase BRI1. *Science* 288, 2360-2363.

Google Scholar: [Author Only](#) [Title Only](#) [Author and Title](#)

Hohmann, U., Nicolet, J., Moretti, A., Hothorn, L.A., and Hothorn, M. (2018a). The SERK3 elongated allele defines a role for BIR ectodomains in brassinosteroid signalling. *Nat. Plants* 4, 345-351.

Google Scholar: [Author Only](#) [Title Only](#) [Author and Title](#)

Hohmann, U., Santiago, J., Nicolet, J., Olsson, V., Spiga, F.M., Hothorn, L.A., Butenko, M.A., and Hothorn, M. (2018b). Mechanistic basis for the activation of plant membrane receptor kinases by SERK-family coreceptors. *Proc. Natl. Acad. Sci. USA* 115, 3488-3493.

Google Scholar: [Author Only](#) [Title Only](#) [Author and Title](#)

Holzwart, E., Huerta, A.I., Glöckner, N., Garnelo Gómez, B., Wanke, F., Augustin, S., Askani, J.C., Schürholz, A-K., Harter, K., and Wolf, S. (2018). BRI1 controls vascular cell fate in the *Arabidopsis* root through RLP44 and phytosulfokine signaling. *Proc. Natl. Acad. Sci. USA* 115, 11838-11843.

Google Scholar: [Author Only](#) [Title Only](#) [Author and Title](#)

Holzwart, E., Wanke, F., Glöckner, N., Höfte, H., Harter, K., and Wolf, S. (2020). A mutant allele uncouples the brassinosteroid-dependent and independent functions of BRASSINOSTEROID INSENSITIVE 1. *Plant Physiol.* 182, 669-678.

Google Scholar: [Author Only](#) [Title Only](#) [Author and Title](#)

Hothorn, M., Belkhadir, Y., Dreux, M., Dabi, T., Noel, J.P., Wilson, I.A., and Chory, J. (2011). Structural basis of steroid hormone perception by the receptor kinase BRI1. *Nature* 474, 467-471.

Google Scholar: [Author Only](#) [Title Only](#) [Author and Title](#)

Irani, N.G., Di Rubbo, S., Myle, E., Van den Begin, J., Schneider-Pizoń, J., Hniliková, J., Šišá, M., Buyst, D., Vilarrasa-Blasi, J., Szatmári, A-M., et al. (2012). Fluorescent castasterone reveals BRI1 signaling from the plasma membrane. *Nat. Chem. Biol.* 8, 583-589.

Google Scholar: [Author Only](#) [Title Only](#) [Author and Title](#)

Jaillais, Y., Belkadir, Y., Balsemão-Pires, E., Dangl, J.L., and Chory, J. (2011). Extracellular leucine-rich repeats as a platform for receptor/coreceptor complex formation. Proc. Natl. Acad. Sci. USA 108, 8503-8507.

Google Scholar: [Author Only](#) [Title Only](#) [Author and Title](#)

Kinoshita, T., Caño-Delgado, A., Seto, H., Hiranuma, S., Fujioka, S., Yoshida, S., and Chory, J. (2005). Binding of brassinosteroids to the extracellular domain of plant receptor kinase BRI1. Nature 433, 167-171.

Google Scholar: [Author Only](#) [Title Only](#) [Author and Title](#)

Lam, S.K., Cai, Y., Tse, Y.C., Wang, J., Law, A.H.Y., Pimpl, P., Chan, H.Y.E., Xia, J., and Jiang, L. (2009). BFA-induced compartments from the Golgi apparatus and trans-Golgi network/early endosome are distinct in plant cells. Plant J. 60, 865-881.

Google Scholar: [Author Only](#) [Title Only](#) [Author and Title](#)

Li, J., Wen, J., Lease, K.A., Doke, J.T., Tax, F.E., and Walker, J.C. (2002). BAK1, an *Arabidopsis* LRR receptor-like protein kinase, interacts with BRI1 and modulates brassinosteroid signaling. Cell 110, 213-222.

Google Scholar: [Author Only](#) [Title Only](#) [Author and Title](#)

Liu, D., Kumar, R., Claus, L.A.N., Johnson, A.J., Siao, W., Vanhoutte, I., Wang, P., Bender, K.W., Yperman, K., Martins, S., et al. (2020). Endocytosis of BRASSINOSTEROID INSENSITIVE1 is partly driven by a canonical Tyr-based motif. Plant Cell 32, 3598-3612.

Google Scholar: [Author Only](#) [Title Only](#) [Author and Title](#)

Luo, Y., Scholl, S., Doering, A., Zhang, Y., Irani, N.G., Rubbo, S.D., Neumetzler, L., Krishnamoorthy, P., Van Houtte, I., Mylie, E., et al. (2015). V-ATPase activity in the TGN/EE is required for exocytosis and recycling in *Arabidopsis*. Nat. Plants 1, 15094.

Google Scholar: [Author Only](#) [Title Only](#) [Author and Title](#)

Luo, Y., Takagi, J., Claus, L.A.N., Zhang, C., Yasuda, S., Hasegawa, Y., Yamaguchi, J., Shan, L., Russinova, E., and Sato, T. (2022). Deubiquitinating enzymes UBP12 and UBP13 stabilize the brassinosteroid receptor BRI1. EMBO Rep. 23, e53354.

Google Scholar: [Author Only](#) [Title Only](#) [Author and Title](#)

Martins, S., Dohmann, E.M.N., Cayrel, A., Johnson, A., Fischer, W., Pojer, F., Satiat-Jeunemaître, B., Jaillais, Y., Chory, J., Geldner, N., and Vert, G. (2015). Internalization and vacuolar targeting of the brassinosteroid hormone receptor BRI1 are regulated by ubiquitination. Nat. Commun. 6, 6151.

Google Scholar: [Author Only](#) [Title Only](#) [Author and Title](#)

Metz, C., Oyanadel, C., Jung, J., Retamal, C., Cancino, J., Barra, J., Venegas, J., Du, G., Soza, A., and González, A. (2021). Phosphatidic acid-PKA signaling regulates p38 and ERK1/2 functions in ligand-independent EGFR endocytosis. Traffic 22, 345-361.

Google Scholar: [Author Only](#) [Title Only](#) [Author and Title](#)

Noguchi, T., Fujioka, S., Choe, S., Takatsuto, S., Yoshida, S., Yuan, H., Feldmann, K.A., and Tax, F.E. (1999). Brassinosteroid-insensitive dwarf mutants of *Arabidopsis* accumulate brassinosteroids. Plant Physiol. 121, 743-752.

Google Scholar: [Author Only](#) [Title Only](#) [Author and Title](#)

Nolan, T.M., Vukašinović, N., Liu, D., Russinova, E., and Yin, Y. (2020). Brassinosteroids: multidimensional regulators of plant growth, development, and stress responses. Plant Cell 32, 295-318.

Google Scholar: [Author Only](#) [Title Only](#) [Author and Title](#)

Oksvold, M.P., Pedersen, N.M., Forfang, L., and Smeland, E.B. (2012). Effect of cycloheximide on epidermal growth factor receptor trafficking and signaling. FEBS Lett. 586, 3575-3581.

Google Scholar: [Author Only](#) [Title Only](#) [Author and Title](#)

Pettersen, E.F., Goddard, T.D., Huang, C.C., Meng, E.C., Couch, G.S., Croll, T.I., Morris, J.H., and Ferrin, T.E. (2021). UCSF ChimeraX: Structure visualization for researchers, educators, and developers. Protein Sci. 30, 70-82.

Google Scholar: [Author Only](#) [Title Only](#) [Author and Title](#)

Russinova, E., Borst, J.-W., Kwaaitaal, M., Caño-Delgado, A., Yin, Y., Chory, J., and de Vries, S.C. (2004). Heterodimerization and endocytosis of *Arabidopsis* brassinosteroid receptors BRI1 and AtSERK3 (BAK1). Plant Cell 16, 3216-3229.

Google Scholar: [Author Only](#) [Title Only](#) [Author and Title](#)

Šali, A. and Blundell, T.L. (1993). Comparative protein modelling by satisfaction of spatial restraints. J. Mol. Biol. 234, 779-815.

Google Scholar: [Author Only](#) [Title Only](#) [Author and Title](#)

She, J., Han, Z., Kim, T.-W., Wang, J., Cheng, W., Chang, J., Shi, S., Wang, J., Yang, M., Wang, Z.-Y., and Chai, J. (2011). Structural insight into brassinosteroid perception by BRI1. Nature 474, 472-476.

Google Scholar: [Author Only](#) [Title Only](#) [Author and Title](#)

Smith, J.M., Salamango, D.J., Leslie, M.E., Collins, C.A., and Heese, A. (2014). Sensitivity to Flg22 is modulated by ligand-induced degradation and de novo synthesis of the endogenous flagellin-receptor FLAGELLIN-SENSING2. Plant Physiol. 164, 440-454.

Google Scholar: [Author Only](#) [Title Only](#) [Author and Title](#)

Ursache, R., Andersen, T.G., Marhavý, P., and Geldner, N. (2018). A protocol for combining fluorescent proteins with histological stains for diverse cell wall components. *Plant J.* 93, 399-412.

Google Scholar: [Author Only](#) [Title Only](#) [Author and Title](#)

von Wangenheim, D., Hauschild, R., Fendrych, M., Barone, V., Benková, E., and Friml, J. (2017). Live tracking of moving samples in confocal microscopy for vertically grown roots. *eLife* 6, e26792.

Google Scholar: [Author Only](#) [Title Only](#) [Author and Title](#)

Wang, X., and Chory, J. (2006). Brassinosteroids regulate dissociation of BKI1, a negative regulator of BRI1 signaling, from the plasma membrane. *Science* 313, 1118-1122.

Google Scholar: [Author Only](#) [Title Only](#) [Author and Title](#)

Wang, Z.-Y., Nakano, T., Gendron, J., He, J., Chen, M., Vafeados, D., Yang, Y., Fujioka, S., Yoshida, S., Asami, T., and Chory, J. (2002). Nuclear-localized BZR1 mediates brassinosteroid-induced growth and feedback suppression of brassinosteroid biosynthesis. *Dev. Cell* 2, 505-513.

Google Scholar: [Author Only](#) [Title Only](#) [Author and Title](#)

Wang, Z.-Y., Seto, H., Fujioka, S., Yoshida, S., and Chory, J. (2001). BRI1 is a critical component of a plasma-membrane receptor for plant steroids. *Nature* 410, 380-383.

Google Scholar: [Author Only](#) [Title Only](#) [Author and Title](#)

Waterhouse, A.M., Procter, J.B., Martin, D.M.A., Clamp, M., and Barton, G.J. (2009). Jalview Version 2-A multiple sequence alignment editor and analysis workbench. *Bioinformatics* 25, 1189–1191.

Google Scholar: [Author Only](#) [Title Only](#) [Author and Title](#)

Wolf, S., Mravec, J., Greiner, S., Mouille, G., and Höfte, H. (2012). Plant cell wall homeostasis is mediated by brassinosteroid feedback signaling. *Curr. Biol.* 22, 1732-1737.

Google Scholar: [Author Only](#) [Title Only](#) [Author and Title](#)

Wolf, S., van der Does, D., Ladwig, F., Sticht, C., Kolbeck, A., Schürholz, A.-K., Augustin, S., Keinath, N., Rausch, T., Greiner, S., et al. (2014). A receptor-like protein mediates the response to pectin modification by activating brassinosteroid signaling. *Proc. Natl. Acad. Sci. USA* 111, 15261-15266.

Google Scholar: [Author Only](#) [Title Only](#) [Author and Title](#)

Yin, Y., Wang, Z.-Y., Mora-Garcia, S., Li, J., Yoshida, S., Asami, T., and Chory, J. (2002). BES1 accumulates in the nucleus in response to brassinosteroids to regulate gene expression and promote stem elongation. *Cell* 109, 181-191.

Google Scholar: [Author Only](#) [Title Only](#) [Author and Title](#)

Yoshinari, A., Hosokawa, T., Amano, T., Beier, M.P., Kunieda, T., Shimada, T., Hara-Nishimura, I., Naito, S., and Takano, J. (2019). Polar localization of the borate exporter BOR1 requires AP2-dependent endocytosis. *Plant Physiol.* 179, 1569-1580.

Google Scholar: [Author Only](#) [Title Only](#) [Author and Title](#)

Zhou, J., Liu, D., Wang, P., Ma, X., Lin, W., Chen, S., Mishev, K., Lu, D., Kumar, R., Vanhoutte, I., et al. (2018). Regulation of *Arabidopsis* brassinosteroid receptor BRI1 endocytosis and degradation by plant U-box PUB12/PUB13-mediated ubiquitination. *Proc. Natl. Acad. Sci. USA* 115, E1906-E1915.

Google Scholar: [Author Only](#) [Title Only](#) [Author and Title](#)

Zhou, Y., and Sakurai, H. (2022). New trend in ligand-induced EGFR trafficking: a dual-mode clathrin-mediated endocytosis model. *J. Proteomics* 255, 104503.

Google Scholar: [Author Only](#) [Title Only](#) [Author and Title](#)